Effects of thermal emission and re-trapping of photo-injected carriers on the optical transitions of InAs/GaAs quantum dots

J. Jawher, Radhwen Chtourou, Vincent Sallet, Mehrez Oueslati

Effects of thermal emission and re-trapping of charged carriers

on the optical transitions of InAs quantum dots under very low excitation density

Rihani Jawher [a,*], Radhwen Chtourou [a], Vincent Sallet [b], Mehrez Oueslati [c]

[a] Laboratoire de Photovoltaïque et des Semiconducteurs, Centre de la Recherche et de Technologie de l'Energie, BP. 95, Hammam-Lif 2050, Tunisia

[b] Groupe d'Etude de la Matière Condensée (GEMAC), CNRS, Université de Versailles St Quentin en Yvelines, Université Paris-Saclay, 45 avenue des Etats-Unis, 78035 Versailles, France

[c] Laboratoire de Nanomatériaux, Nanotechnologie et Energie (L2NE), Faculté des Sciences de Tunis, Université de Tunis El Manar, 2092 Tunis, Tunisia

Abstract:

Photoluminescence (PL) measurements are presented for self-assembled InAs/GaAs quantum dots (QDs) grown by molecular beam epitaxy (MBE) at a growth temperature of 510°C. Two well-defined sub-bands were observed from the 8K-PL spectrum obtained under very low excitation density and unambiguously clarified as optical emissions from the ground state (GS) and first excited state (FES) of the dots. Temperature-dependent PL measurements were investigated in the 8-270K temperature range. Differently from the FES transition, a sigmoidal temperature-dependent variation was observed from the integrated PL intensity of the GS transition. This anomalous behavior was assigned to the carrier exchange between excited states and GS of the dots. A simple rate equation model which takes into account the effects of the thermal escape and re-trapping of photo-injected carriers was proposed to describe the temperature-dependent variation of the integrated PL intensity. A good agreement between the model simulation and the experimental results was obtained for temperatures ranging from 8 to 270K and which supports the argument for the carrier exchange between the excited states and the ground state.

∗Corresponding author. Tel. : +21697669764 ; fax : + 79325825.

E-mail address: rihani_jaouher@yahoo.fr

1. Introduction:

Semiconductor-based quantum dots produced by self-organized growth are the subject of intensive studies due to their potential employ in the optoelectronic area as well as in the manufacture of intermediate band solar cells [1-4]. Theoretical works correlating the energy states to the dot's size have been largely reported in the literature of InAs/GaAs QDs system [5, 6]. The energy spacing between two consecutive states of the QD exceeds the thermal energy k_BT and therefore the optical transitions from the excited states are clearly visible even at high temperature [7]. However, additional sub-bands arising from the size fluctuations of the dots could appear in one PL spectrum of InAs QDs ensemble. Indeed, a large number of dots ($10^4 \sim 10^7 . mm^{-2}$) is excited in the PL experiments [7, 8]. So, if the sample contains several families of dots, then their corresponding emission bands should appear in the PL spectrum. Now, it is well established data that the increase of the PL measurement temperature in such structure has to show some abnormal behaviors in their PL characteristics. These abnormal behaviors are the signature of several ways of carrier redistribution within the QD structure [9-14]. The thermal redistribution of carriers in this QD structure could result from the thermal release of excitons trapped in narrowing potentials [9, 10] and also from the thermal transport of carriers from the ground states of small QDs into lower-lying states of larger dots [11-14]. However, only a few works have reported carrier exchange mechanisms between the excited states and the GS of the QDs from temperature-dependent PL investigations [15-17]. In reference [15], Levesque et al. have shown from yhe optical study of vertically aligned InAs/InP QDs that the first excited states could be repopulated via a thermal escape of carriers coming from the ground states. Once in the excited states, the carriers could relax in deeper states or lost through nonradiative recombination paths (dark excited states). On the other hand, from optical measurements of InAs QDs system, the authors in Ref [16] have attributed the abnormal dependence on the temperature of the PL linewidth to the direct repopulation of the QD excited states by carriers thermally emitted from the ground states. In this reported work, the repopulated excited states do not act as dark excited states (*DES*) since the intensity ratio between the excited-state and the ground-state transitions has increased with the increase of the temperature. As a result, the thermal redistribution of carriers has been demonstrated to introduce significant changes in the optical properties of self-assembled QDs system.

In this work, PL measurements as function of the temperature were carried out self-assembled InAs/GaAs QDs. An anomalous temperature-dependent variation was observed in

the integrated PL intensity of the GS emission at relatively low temperatures. A rate equation model was proposed to interpret the unusual dependence on the temperature of the integrated PL intensity. The model takes into account the effects of the thermal escape and re-trapping of charged carriers in the excited states of the InAs/GaAs QDs.

2. Experimental details:

The studied structure in this work contains a single InAs QD layer sandwiched in a GaAs matrix [18]. Stranski-Krastanov InAs QDs were grown on a semi-insulating GaAs (001)-oriented by conventional solid source MBE. Gallium and indium fluxes were supplied from thermal effusion cells, As_2 species from a cracking source. The growth procedure for the QD deposition was the following. First, a 0,3 μm thickness of the GaAs buffer was grown at 600°C with a rate of 0,2 nm/s. Before the end of the GaAs buffer, the substrate temperature was decreased to 510°C in order to allow the deposit of the wetting layer (WL). The thickness of the InAs deposited and the growth rate were fixed to 2,8 monolayers and 0,04 nm/s respectively. Then, the growth temperature was increased to reach again 600°C and a 0,1 μm thickness of the GaAs cap was immediately deposited. Another sample was grown for the atomic force microscope (AFM) measurements using the same conditions, but without the cap layer. Morphology analysis was performed using the tapping mode of a Topometrix *TMX 2000* Explorer atomic force microscope. PL measurements were carried out using a closed-cycle He cryostat and a 514.5-nm line of an Ar^+ laser. Optical spectra were collected with a $f = 0{,}25$ m spectrometer with a 1200 l/mm grating and focused onto a cooled GaInAs photodiode detector.

3. Results and discussion:

3.1. Structural details:

Fig. 1a shows the AFM image of the uncapped QD sample and Fig. 1b exhibits the corresponding lateral size histogram of the dots. The structural details of the dots within the sample are summarized in Table 1. AFM image clearly shows a good uniformity of dots in terms of shape and size. Fig. 1b clearly demonstrates the monomodal size distribution of dots within the studied sample. The microscopic analysis performed on the dots provide an average diameter of a about 22 nm, ~ 4 nm in height and an area density of around $3{,}6 \times 10^{10}$ cm^{-2} (see Tab. 1).

3.2. Photoluminescence at 8K:

The 8K-PL spectrum of the investigated sample under very low pump excitation power (of around 0,04 $W.cm^{-2}$) is shown in Fig. 2a. This spectrum exhibits two well-defined sub-bands (S and P). The energy spacing between their peak positions is around 28 meV. Referring to the structural details which demonstrate quite homogeneous dots, the S and P bands are related to the ground-state and first excited-state transitions of the dots, respectively [4-6]. This assumption is supported by the pump power-dependent optical measurements (see Fig. 2b) which show significant changes in the overall shape of the PL spectra. Indeed, the PL spectra of Fig. 2b mark the emergence of new emission lines in the high energy side when the excitation density is increased. The new lines result from the exciton occupations at different atom-like shells in the quantum dots and are attributed to the radiative recombination from populated excited states even when the ground states are far from saturation. However, similar optical observations of the PL emission from the first excited state using an extremely low excitation density (~ 0,04 $W.cm^{-2}$) are rarely available in the literature [19, 20]. The appearance of the optical emission from populated excited states when the fundamental states are far from saturation has been related to the slow relaxation of carriers across the QD levels [20]. The line-width recorded from the 8K-PL spectrum (Fig. 2a) is around of 32 meV. Such value is too small in comparison with the usually reported (~ 50 meV) for such QD structure [4, 11] and which confirms the high uniformity of the dots size within the sample.

3.3. PL as a function of the temperature:

Temperature-dependent PL measurements of the sample were carried out by varying the temperature from 8 to 270K, as shown in Fig. 3. **The continuous pump power was maintained at extremely low excitation density (of about 0,04 W/cm²) which corresponds to approximately $1,04 \times 10^9$ e-h pairs per square centimeter. Taking into account the structural results of the sample, the average dot occupancy is estimated at approximately 0,03 e-h pairs per QD.** Such QD occupancy is adequately enough to neglect the many-body interaction effects such as bi-excitonic optical recombination, Auger scattering and band gap renormalization [21, 22]. Each spectrum of figure 3 is well fitted by a Gaussian deconvolution into S and P sub-bands. The exact values of the emission energies (dubbed E_S and E_P), the line widths (dubbed $FWHM_S$ and $FWHM_P$, respectively) and the integrated PL intensities (dubbed $IPLI_S$ and $IPLI_P$, respectively) are extracted from fitting results. The variations of E_S, E_P, $FWHM_S$, $FWHM_P$, $IPLI_S$, and $IPLI_P$ with the increase of the temperature are represented in Fig. 4. The evolution of the InAs band gap with the increase of the temperature (calculated according to the Varshni law [23]) is plotted in Fig. 4a using the

parameters of bulk InAs [23]. The InAs band gap is shifted along the energy axis of 740 meV and 768 meV for the GS and FES transitions, respectively.

The peak energy change of the FES emission nicely follows the variation of the bulk InAs band gap over the whole temperature range (see Fig. 4a). This behavior indicates that the thermal carrier transfer via neighboring QDs is probably not prominent in the studied structure [11, 24]. Indeed, no signature of rapid redshifting behavior with respect to the InAs band gap was detected from the temperature dependence of the FES emission energy. While the peak energy of the GS emission exhibits a deviation from the bulk InAs band gap change from a temperature of about 120K (see Fig. 4a). The deviation from the InAs band gap is attributed to the preferential thermal quenching of the PL signal from the shallower confinement states of the dots when the temperature is increased [24]. Meanwhile, Fig. 4c and Fig. 4d show that the integrated intensities of the two sub-bands exhibit non-common quenching behaviors when the temperature is increased from 8K till 120K. While, above this temperature, the QD radiative transitions show a strong quenching behavior. Such variations of the integrated intensity and peak energy indicate that there are two regimes characterizing the thermal quenching of the GS transition when the temperature is increased from 8 to 270K. The first one occurs in the 8-120K temperature range (first regime) and the second one occurs above 120K (second regime). This assumption is supported by the variation of the $FWHM_S$ (see Fig. 4b) which shows a slight increase in the 8-120K temperature range followed by a strong reduced broadening for temperatures above 120K. The variations of the PL characteristics of the GS transition vs temperature present very interesting behaviors and will be discussed later. We discuss now the PL characteristics of the FES transition.

Fig. 4d shows that the integrated intensity of the FES transition exhibits a monotone quenching behavior with the increase of the temperature. The data can be nicely fitted with the Arrhenius formula [25] (Eq. I) over the whole studied temperature range. Another careful fitting was performed on the same data using the relationship [26] (Eq. II):

$$I_P(T) = \frac{I_P(0)}{1 + L_1 \times T^{3/2} + L_2 \times T^{1/2} \exp\left(-\frac{e_P}{kT}\right)} \qquad \text{Eq. I}$$

$$I_P(T) \propto \frac{I_P(0)}{\left\{1 + L_p \,.\, exp(-e_P/kT)\right\}^2} \qquad \text{Eq. II}$$

where L_1, L_2, L_P and e_P are the fitting parameters and $I_P(0) \approx I_P(8K)$. The fitting results obtained from the fit to the data using both Eq. I and Eq. II laws are summarized in Table 2. These results show the same activation energy (e_P) of the FES transition obtained with the use

of both Eq. I and Eq. II relationships. The small value of e_P (of about 52 meV) should not be assigned to a thermal escape of carriers outside the dot barrier towards the WL and/or GaAs bulk states [7, 14]. The value of e_P is very close to the energy spacing (of about 51 meV at 8K) between d-shell and p-shell transitions (see Fig. 2b). Thus, the thermal quenching of the FES transition can be explained by the thermal emission of carriers from the first excited state towards the second excited state of the dots that act as nonradiative levels (dark excited states) [15, 17].

With increasing temperature, the evolutions of the PL characteristics of the GS transition are governed by two regimes. In the low temperature regime (below 120K), it can be clearly seen from Fig. 4c that the integrated PL intensity exhibits a sigmoidal temperature-dependent variation ("knee feature") which indicates a typical behavior of carrier redistribution within the QD structure. Indeed, with increasing temperature from 8K to 50K the $IPLI_S$ slowly decreases, then remains constant till 70K, and decreases again but much faster with a further increase in the temperature. This sigmoidal dependence of the integrated PL intensity implies a non-typical thermal quenching of the GS transition compared to that of the FES one. In the first regime (see Fig. 4c), the constant variation of the $IPLI_S$ suggests that the thermal escape of carriers was compensated by some mechanism providing carriers to the ground states of the dots. Such a mechanism should have an influence only on the quenching behavior of the GS transition and moreover, it should have a minor impact in the second regime (above 120K).

Several possible mechanisms have been proposed for InAs QD structures to account for the enhancement of the PL signal with the increase of the temperature [9-16]. The mechanisms that have evidenced a redistribution of carriers between neighboring dots (inter-dot carrier redistribution mechanism) cannot be considered in the present optical results. This is supported by the dependence on temperature of the emission energy of the FES, which has revealed that such mechanisms are almost improbable. On the other hand, these mechanisms occur in the intermediate temperature range (above ~140K) for structures owing different size distributions of dots and/or low surface densities of dots (of around $10^7 \sim 10^8\ cm^{-2}$) [11-14], which is not the case of the present experiments. The mechanisms involving the thermal release of electrons from traps located in the barriers [9, 10] could not apply also in the present case since these mechanisms should enhance the PL signals of both GS and FES transitions. However, the mechanisms describing a redistribution of carriers between the excited states and the GS of the dots (intra-dot carrier redistribution mechanism) could be

considered in the present case since the FES is believed to populate the *DES* via thermal escape of carriers [15-17]. On the other hand, Fig. 4 shows that the sigmoidal dependence of the $IPLI_S$ coincides with the reduced broadening evolution of the $FWHM_P$ and also, at the same time, coincides with the broadening evolution of the $FWHM_S$. All the coincidences occur in the low quenching regime (first regime) should therefore involve correlated phenomena. Note that the shrinkage of the $FWHM_P$ with the increase of the temperature is contrary to that expected for self-assembled QDs structures [24, 27]. Indeed, for InAs QDs system, the increase of the PL measurement temperature causes a broadening of the inter-band radiative transitions. This is due to the carrier-phonon scattering process (homogeneous broadening) and also due to the non-homogeneity of the dots size within the sample (inhomogeneous broadening). However, for such systems, the narrowing of the PL signal with the increase of the temperature has been clarified as a result of the thermal redistribution of carriers within the QDs structure. Since the anomalous behavior of the $IPLI_S$ variation coincides with the unexpected decrease of the $FWHM_P$, the sigmoidal dependence of the $IPLI_S$ (see Fig. 4) is therefore related to the carrier exchange between the FES and the GS [16]. On the other hand, considering the above assignment concerning the thermal emission of carriers from FES to *DES*, the supply of carriers to the GS is therefore believed to be arising from a re-capture of carriers from the *DES*. This assignment is supported by the ultra-short relaxation process of carriers through the sublevels of the dots (in the ps range) compared to that of the carrier recombination (in the ns range) [17, 28, 29].

3.4 Model description and discussion:

In order to verify our reasoning, a simple rate equation model is proposed to describe the carrier relaxation dynamics in the investigated structure. The charge carrier movements are schematically described in Fig. 5. As cited above, even at extremely low excitation density, both GS and FES are populated. In continuous excitation mode, G_0 carriers per QD per second are generated in the bulk GaAs and then fall in the WL barrier. Once in the WL, the carriers are randomly captured either in the GS (with a capture rate of T_S) or in the FES states (with a capture rate of T_P). In the present measurements, the barriers are assumed to acting as transient levels that will provide the carriers without any loss since the PL spectra did not reveal any characteristic bands of emission from the bulk and WL barriers. This means that the capture time to the QD is much faster than the recombination rate in the barrier. The carriers captured by the GS and the FES can spontaneously recombine with radiative recombination rates of R_S and R_P, respectively. With the increase of the temperature,

the carriers injected into the GS and the FES get lost by non-radiative paths with nonradiative recombination rates of $B_S(T)$ and $B_P(T)$, respectively. Taking into account the dark excited states introduced above, the excited states of the QD (with the exception of the FES) are grouped into a subset (*DES*) which will acquire the thermally escaped carriers coming from the FES. Once in the *DES*, the carriers can be re-captured by the GS with a capture rate of T_D or get lost by non-radiative paths with a nonradiative recombination rate of N_R. The terms describing the thermal emission of carriers from the GS and FES are $B_S(T) = \Gamma_S \exp\left(-\frac{e_S}{kT}\right)$ and $B_P(T) = \Gamma_P \exp\left(-\frac{e_P}{kT}\right)$, respectively. e_S and e_P are the needed activation energies for carriers to escape from the GS and FES, respectively. The correlation between carriers involved in the capture and in the thermal emission processes was neglected. This assumption is justified by the very low excitation density used in the present experiments which should probably not involve many-body interaction effects [21]. The charge carrier movements under steady state conditions are as follows:

Barriers: $$G_0 - T_S n_B - T_P n_B = \frac{dn_B}{dt} = 0 \quad (1)$$

So : $$G_S = T_S n_B = \frac{T_S}{T_S+T_P}.G_0 \quad \text{and} \quad G_P = T_P n_B = \frac{T_P}{T_S+T_P}.G_0 \quad (2)$$

Where G_0, G_S and G_P are the generation rates of carriers in the barriers, FES and GS, respectively.

FES: $$G_P - R_P n_P(T) - B_P(T) n_P(T) = \frac{dn_P}{dt} = 0 \quad (3)$$

DES: $$B_P(T) n_P(T) - T_D n_D(T) - N_R n_D(T) = \frac{dn_D}{dt} = 0 \quad (4)$$

GS: $$G_S - R_S n_S(T) - B_S(T) n_S(T) + T_D n_D(T) = \frac{dn_S}{dt} = 0 \quad (5)$$

Eq. (3) can be transformed into: $$n_P(T) = \frac{G_P}{R_P+B_P(T)}$$

The integrated PL intensity of the FES transition can be given as:

$$I_P(T) = \frac{R_P}{\{R_P + B_P(T)\}} \times n_P(T) = \frac{G_P R_P}{\{R_P + B_P(T)\}^2} = \frac{G_P R_P}{\{R_P + \Gamma_P \, exp(-e_P/kT)\}^2} = \frac{G_P/R_P}{\left\{1+\frac{\Gamma_P}{R_P} exp(-e_P/kT)\right\}^2}$$

So : $$I_P(T) \propto \frac{I_P(8K)}{\{1+ L_P \, . \, exp(-e_P/kT)\}^2} \quad \text{Eq. II}$$

Where $G_P = I_P(0K) \approx I_P(8K)$, $L_P = \frac{\Gamma_P}{R_P}$ and e_P are the fitting parameters that have already been obtained from the fit of the $IPLI_P$ data with the help of the Eq. II law (Table 2). The fitting parameters are $L_P = \frac{\Gamma_P}{R_P} \approx 26{,}3 \pm 1{,}64$ and $e_P = 52 \pm 1{,}3\ meV$.

Eq. (4) can be transformed into: $$n_D(T) = \frac{B_P(T) n_P(T)}{T_D + N_R} = \frac{G_P}{T_D + N_R} \times \frac{B_P(T)}{R_P + B_P(T)} \quad (6)$$

Eq. (5) transforms into: $$n_S(T) = \frac{G_S + T_D n_D(T)}{R_S + B_S(T)}$$

The integrated PL intensity of the GS transition can be given as:

$$I_S(T) = \frac{R_S}{\{R_S + B_S(T)\}} \times n_S(T) = \frac{R_S \{G_S + T_D n_D(T)\}}{\{R_S + B_S(T)\}^2} \quad (7)$$

By combining Eqs. (6) and (7), the integrated PL intensity of GS can be written as:

$$I_S(T) = \frac{G_S/R_S}{\left\{1 + \frac{\Gamma_S}{R_S}.exp(-e_S/kT)\right\}^2} \times \left\{1 + \frac{G_P}{G_S} \times \frac{T_D/(T_D + N_R)}{1 + \frac{R_P}{\Gamma_P}.exp(e_P/kT)}\right\} \quad (8)$$

Taking into account that (see Tab. 2) $\frac{R_P}{\Gamma_P} = \frac{1}{L_P} \cong 0{,}038$, $e_P \cong 52\ meV$, $\frac{G_P}{G_S} \approx \frac{I_P(0K)}{I_S(0K)} = 0{,}27$ and $I_S(0K) \approx I_S(8K)$, so the $IPLI_S$ data could be fitted with the following law :

$$I_S(T) \propto \frac{I_S(0K)}{\{1 + L_S.exp(-e_S/kT)\}^2} \times \left\{1 + \frac{G_P}{G_S} \times \frac{A}{1 + \frac{1}{L_P}.exp(e_P/kT)}\right\} \quad \text{Eq. III}$$

Where $L_S = \frac{\Gamma_S}{R_S}$, $A = T_D/(T_D + N_R)$ and e_S are the fitting parameters. The best fit is obtained with the following values: $A = 4{,}55 \pm 0{,}06$, $L_S = 0{,}58 \pm 0{,}11$ and $e_S = 11\ meV \pm 1{,}4\ meV$ (see Tab. 2).

Figure 6 exhibits the fit of the experimental data with the help of the Eq. III law. The fit to the Arrhenius formula of the experimental data is also added to this figure. It is clearly obvious from Fig. 6 that the Arrhenius formula cannot explain the abnormal temperature dependence of the $IPLI_S$. However, the Eq. III reproduces the experimental data quite well and therefore confirms all of the above assumptions. Thus, the mechanism of the thermal exchange between excited states and GS provides a good description for the present optical results. In fact, with increasing temperature from 8 till 120K, the carriers are gradually activated from the FES towards the dark excited states. Once in the *DES*, carriers are re-captured by the GS which results in a sigmoidal variation in their integrated PL intensity, a

broadening of their PL signals and a strong narrowing of the first excited-state transition (see Fig. 4). With further increase of the temperature (second regime), the integrated intensity of the GS and the FES transitions show strong quenching behavior which is due to the strong activation of nonradiative recombination paths. The activation energy e_S could be assigned to non-radiative centers located in the vicinity of the dots [14]. e_S could correspond also to a re-population of the FES since the strong quenching regime marks a shrinkage of the $FWHM_P$ which coincides with broadening of the $FWHM_S$ (see Fig. 4b) [16].

4. Conclusion:

Temperature-dependent PL measurements of InAs/GaAs quantum dots were presented. Two bands were detected in the PL spectra from the studied sample and were attributed to the optical emission from the ground state and the first excited state of the dots. The PL characteristics of the GS and FES transitions have shown unusual temperature dependence. The PL intensity of the GS transition is discussed in terms of thermal exchange of carriers between excited states and ground state of the dots. A rate equation model that includes the effects of the thermal emission and re-trapping of photo-injected carriers was proposed to justify the made interpretations. The good agreement between the model simulation and the experimental data has supported the argument for the carrier exchange between the excited states and the ground state of the dots.

References:

[1]: J. Wu, S. Chen, A. Seeds, and H. Liu, J. Phys. D: Appl. Phys. 48, 363001 (2015).

[2]: Xiang-Bin Su, Ying Ding, Ben Ma, Ke-Lu Zhang, Ze-Sheng Chen, Jing-Lun Li, Xiao-Ran Cui, Ying-Qiang Xu, Hai-Qiao Ni, and Zhi-Chuan Niu, Nanoscale Research Letters. 13, 59 (2018).

[3]: Sushant Ghimire and Vasudevanpillai Biju, Journal of Photochemistry and Photobiology C: Photochemistry Reviews Vol 34, P: 137-151(2018).

[4]: R. Heitz, I. Mukhametzhanov, A. Madhukar, A. Hoffmann, and D. Bimberg, Journal of Electronic Materials 28**,** 520-527, (1999).

[5]: O. Gunawan, H. S. Djie, and B. S. Ooi, Phys. Rev. B. 71*,* 205319 (2005).

[6]: Y. H. Zhu, X. W. Zhang, and J. B. Xia, Phys. Rev. B. 73*,* 165326 (2006).

[7]: E. C. Le Ru, J. Fack, and R. Murray, Physical Review B 67, 245318 (2003).

[8]: B. Ohnesorge, M. Albrecht, J. Oshinowo, A. Forchel and Y. Arakawa, , Phys. Rev. B. 54, 11532 (1996).

[9]: Dan P Popescu, Peter G Eliseev, Andreas Stintz, and Kevin J Malloy, Semicond. Sci. Technol. Vol 19, No 1, 33-38 (2003).

[10]: W. H. Jiang, X. L. Ye, B. Xu, H. Z. Xu, D. Ding, J. B. Liang, and Z. G. Wang, J. Appl. Phys. 88, 2529 (2000).

[11]: H. Kissel, U. Müller, C. Walther, and W. T. Masselink, Phys. Rev. B. Vol 62, No 11, 7213 (2000).

[12]: J. Rihani, V.Sallet, N.Yahyaoui, J.C.Harmand, M.Oueslati, and R.Chtourou, Journal of Luminescence, 129, 251–255, (2009).

[13]: Yu. I. Mazur, J. W. Tomm, G. G. Tarasov, H. Kissel, C. Walther, Z. Ya. Zhuchenko, and W. T. Masselink, Physica E, Vol. 13, Issue 2, p. 255-258, (2002).

[14]: G. Saint-Girons and I. Sagnes, J. Appl. Phys. Vol 91, No 12, 10115 (2002).

[15]: A. Lévesque, P. Desjardins, R. Leonelli, and R. A. Masut, Phys. Rev. B. 83, 235304 (2011).

[16]: X. L. Zhou, Y. H. Chen, X. L. Ye, Bo Xu, and Z. G. Wang, Journal of Applied Physics, Vol. 109, 113540 (2011).

[17]: Anna Vinattieri, Marian Zamfirescu, Massimo Gurioli, Marcello Colocci, Stefano Sanguinetti, and Richard Noetzel, phys. stat. sol. (a) 202, No. 14, 2604–2608 (2005).

[18]: V. Sallet, G. Patriarche, O. Mauguin, L. Largeau, and L. Travers, phys. stat. sol. (c) 3, No. 11, 3997–4000 (2006).

[19]: M. Grundmann and D. Bimberg, Phys. Rev. B. 55, 9740 (1997).

[20]: Wei Yong-Qiang, Liu Hiu-Yun, Chai Chun-Lin, Xu Bo, Ding Ding, and Wang Zhan-Guo, Chin. Phys. Lett, Vol. 18 Issue (7): 982-985 (2001).

[21]: R. Heitz, F. Guffarth, I. Mukhametzhanov, A. Madhukar, and D. Bimberg, Phys. Rev. B. 62, 16881 (2000).

[22]: G. Saint-Girons, N. Chauvin, and I. Sagnes, Appl. Phys. Lett. 88, 133101 (2006).

[23]: Y. P. Varshni, Physica (Amesterdam) 34, 149 (1967).

[24]: S. Sanguinetti, M. Henini, M. Grassi Alessi, M. Capizzi, P. Frigeri, and S. Franchi, Phys. Rev. B 60, 8276 (1999).

[25]: Mukul C. Debnath, Baolai Liang, Ramesh B. Laghumavarapu, Guodong Wang, Aparna Das, Bor-Chau Juang, and Diana L. Huffaker, Journal of Applied Physics, 121, 214304 (2017).

[26]: D. Vignauda, X. Wallart, F. Mollot, and B. Sermage, Journal of Applied Physics, Vol. 84, No. 4, 2138-2145 (1998).

[27]: B. Urbaszek, E. J. McGhee, M. Kruger, R. J. Warburton, K. Karrai, T. Amand, B. D. Gerardot, P. M. Petroff, and J. M. Garcia, Phys. Rev. B. 69, 035304 (2004).

[28]: R. Ferreira and G. Bastard, Appl. Phys. Lett. 74, 2818 (1999).

[29]: I. A. Larkin and A. Vagov, Advances in Condensed Matter Physics, Vol. 10, 1-6 (2017).

Figure captions

Figure 1: (a): $0{,}85 \times 0{,}85\ \mu m^2$ image AFM of the uncapped QD sample. **(b):** The lateral size distribution of the dots corresponding to the AFM image.

Figure 2: (a): 8K-Photoluminescence spectrum of the QD sample recorded at very low excitation density (0,04 $W.cm^{-2}$). **(b):** 8K-PL spectra of the sample taken at different excitation densities.

Figure 3: PL spectra of the sample recorded at different temperatures. The measurement excitation density was fixed at 0,04 $W.cm^{-2}$.

Figure 4: (a): Evolution of the PL Peak position for both GS and FES transitions as function of the temperature. The bulk InAs band gap change is shifted according to the Varshni law along the energy axis of 740 meV and 768 meV for the GS and FES transitions, respectively. **(b):** Temperature dependence of the PL line-width from the GS and the FES transitions. **(c):** The experimental PL-integrated intensity of the GS emission vs temperature accompanied with the fit to the Arrhenius law. **(d):** The experimental PL-integrated intensity of the FES transition vs temperature accompanied with the fits to the laws described in the text.

Figure 5: Schematic representation of the energy band diagram of the studied structure. The diagram includes the different carrier movements considered for the rate equation model.

Figure 6: The experimental integrated intensity of the GS transition vs temperature accompanied with both the Arrhenius plot and the fit to the model described in the text.

Table captions

Table 1: Structural parameter values of the investigated QD sample. $\bar{\sigma}$ is the area density, $\bar{d}$ is the average diameter and $\bar{h}$ is the average height of the dots.

Table 2: Parameters obtained from fitting results of the PL experimental data using the models described in the text.

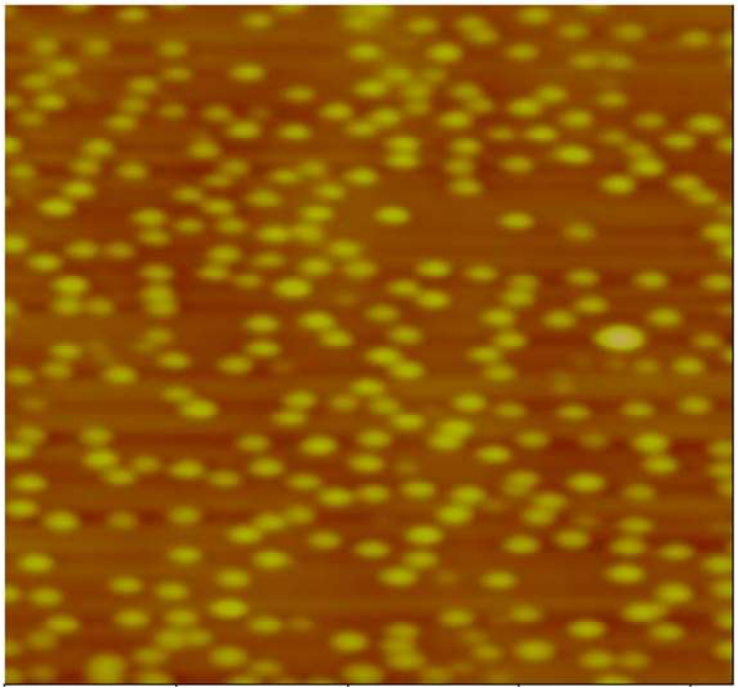

Figure 1: (a): $0{,}85 \times 0{,}85\ \mu m^2$ image AFM of the uncapped QD sample.

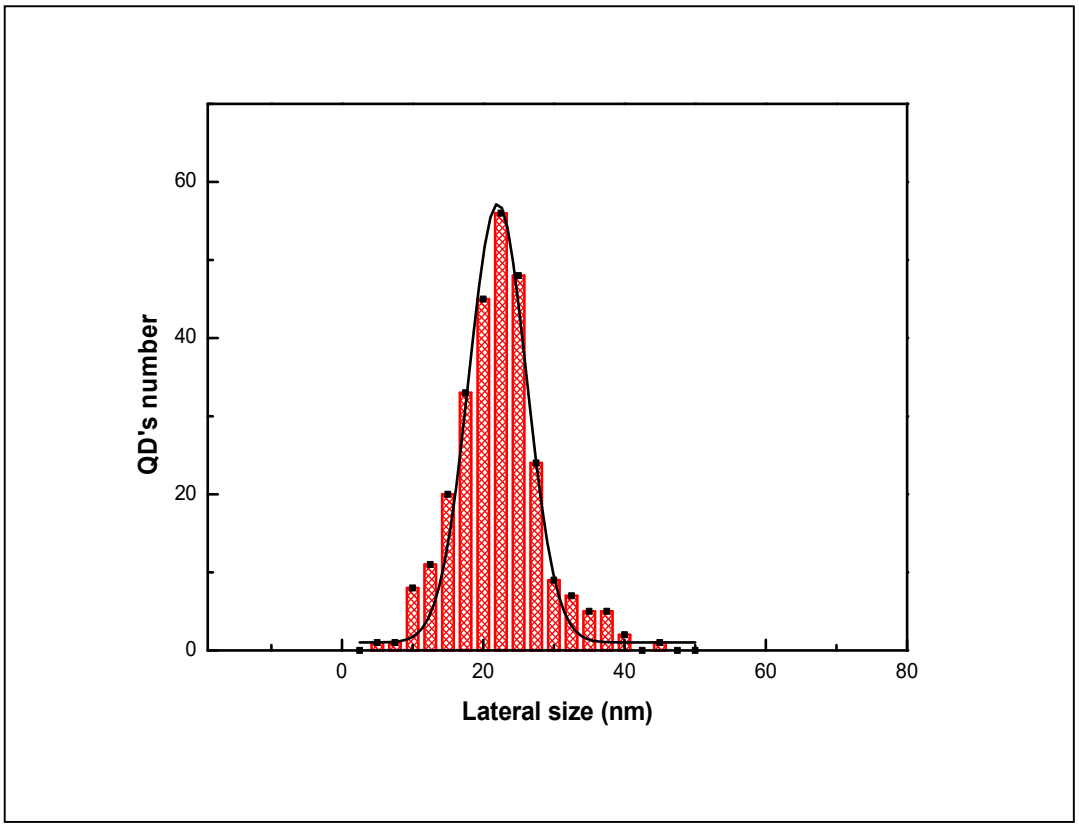

Figure 1b

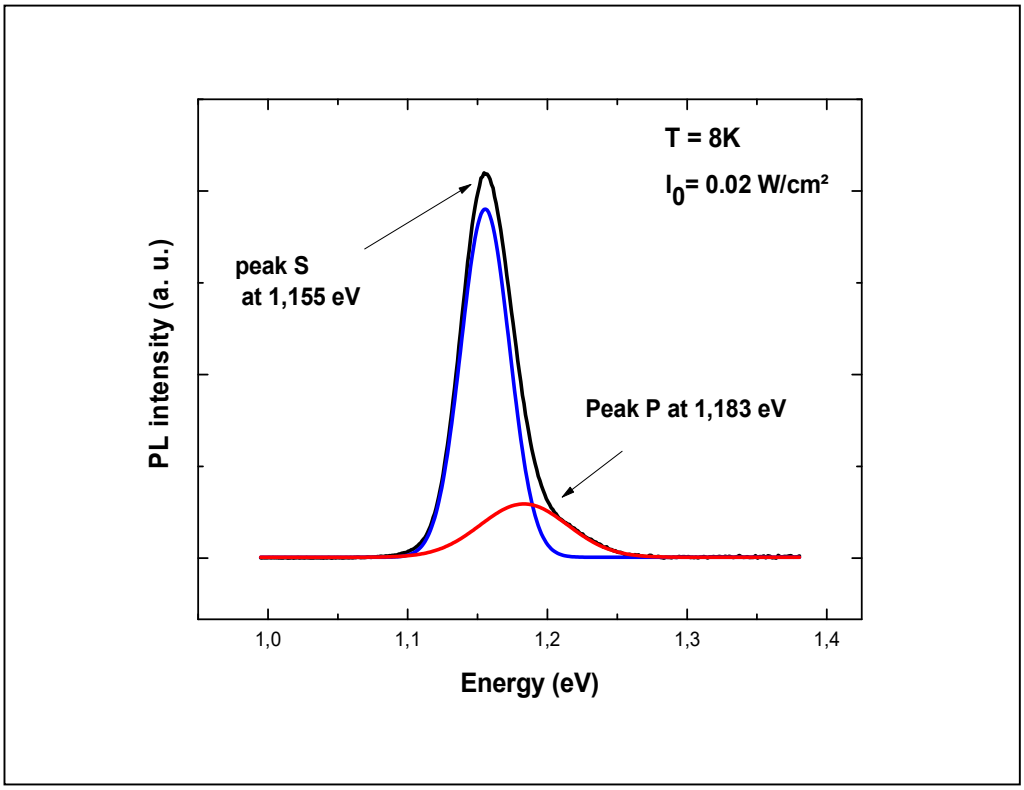
T = 8K
I_0= 0.02 W/cm²
peak S
at 1,155 eV
Peak P at 1,183 eV
PL intensity (a. u.)
1,0
1,1
1,2
1,3
1,4
Energy (eV)

Figure 2a

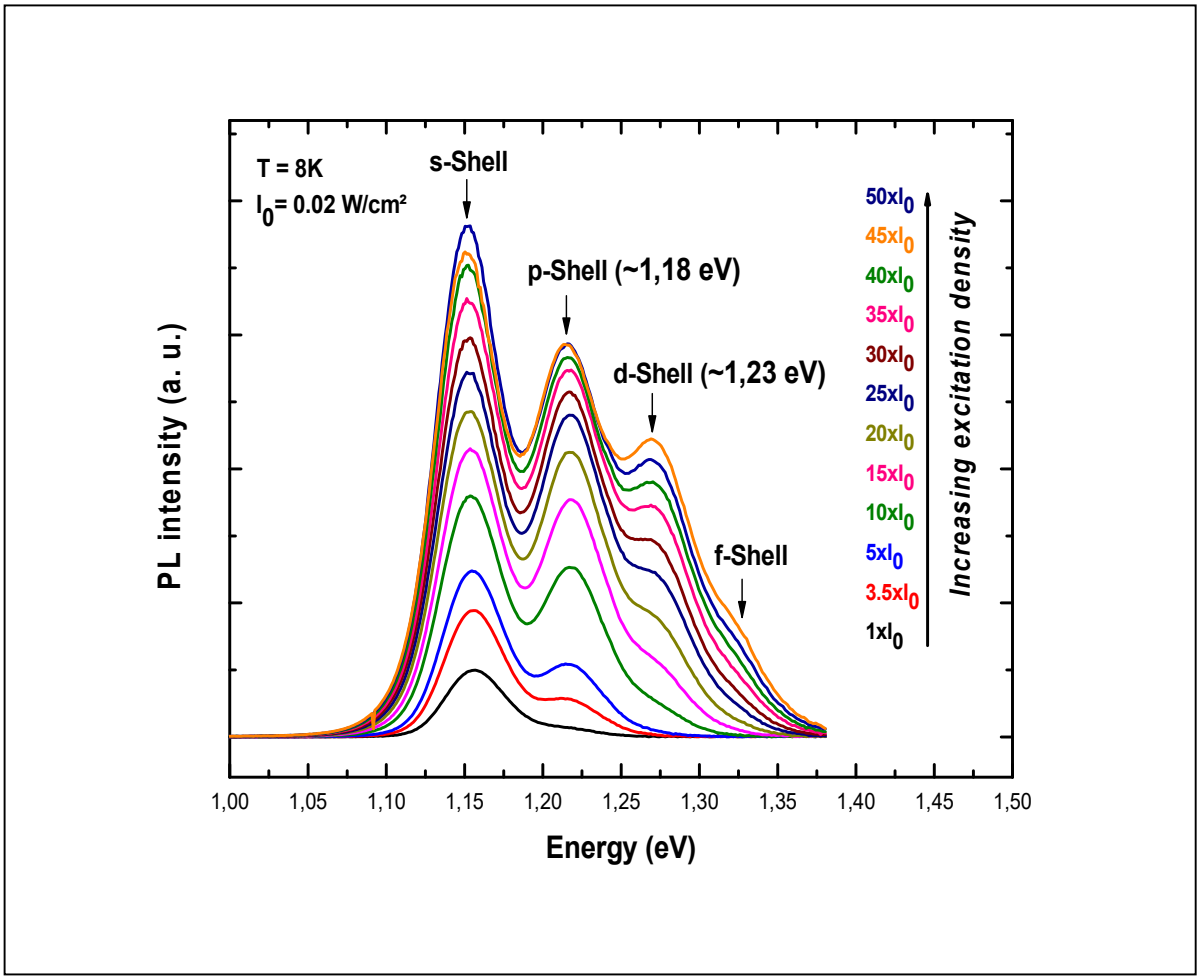
T = 8K
I0= 0.02 W/cm²
s-Shell
p-Shell (~1,18 eV)
d-Shell (~1,23 eV)
f-Shell
50xI0
45xI0
40xI0
35xI0
30xI0
25xI0
20xI0
15xI0
10xI0
5xI0
3.5xI0
1xI0
Increasing excitation density
PL intensity (a. u.)
1,00
1,05
1,10
1,15
1,20
1,25
1,30
1,35
1,40
1,45
1,50
Energy (eV)

Figure 2b

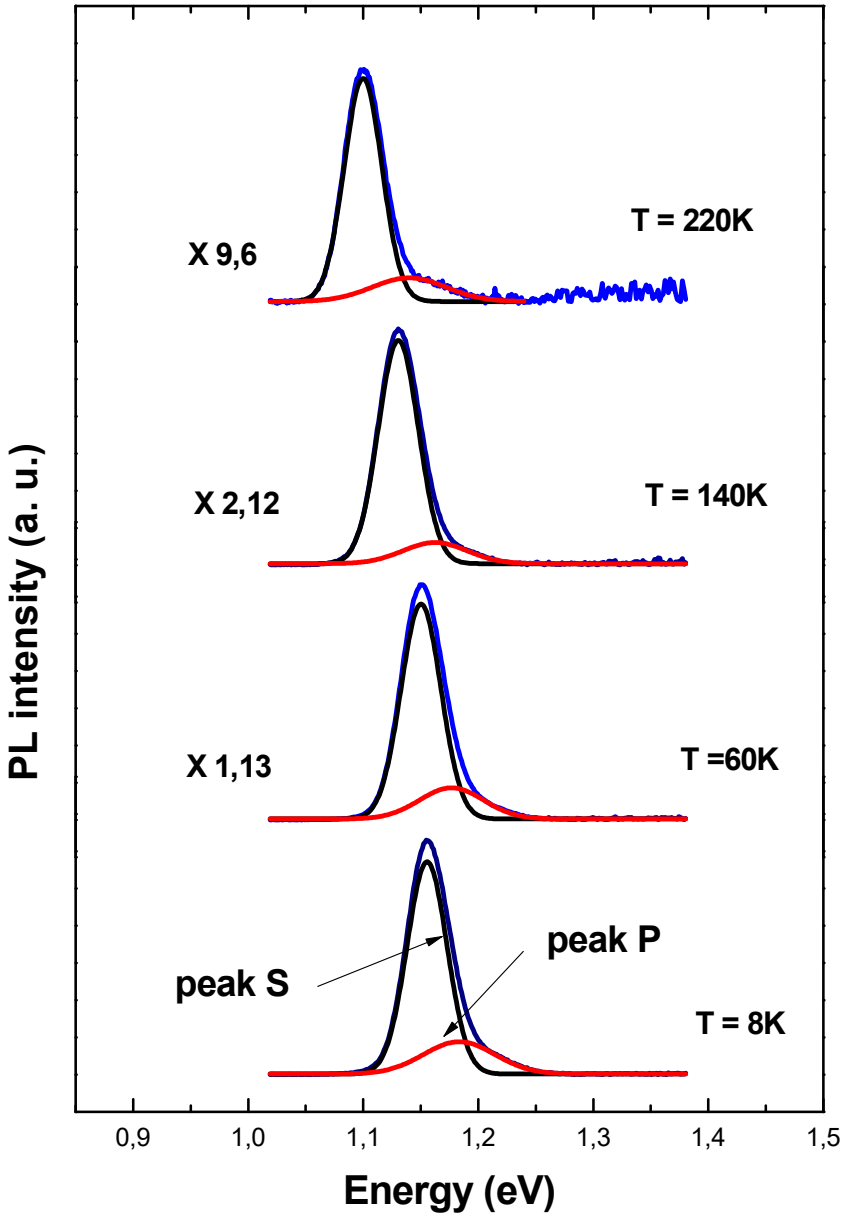
PL intensity (a. u.)
X 9,6
T = 220K
X 2,12
T = 140K
X 1,13
T =60K
peak S
peak P
T = 8K
0,9
1,0
1,1
1,2
1,3
1,4
1,5
Energy (eV)

Figure 3

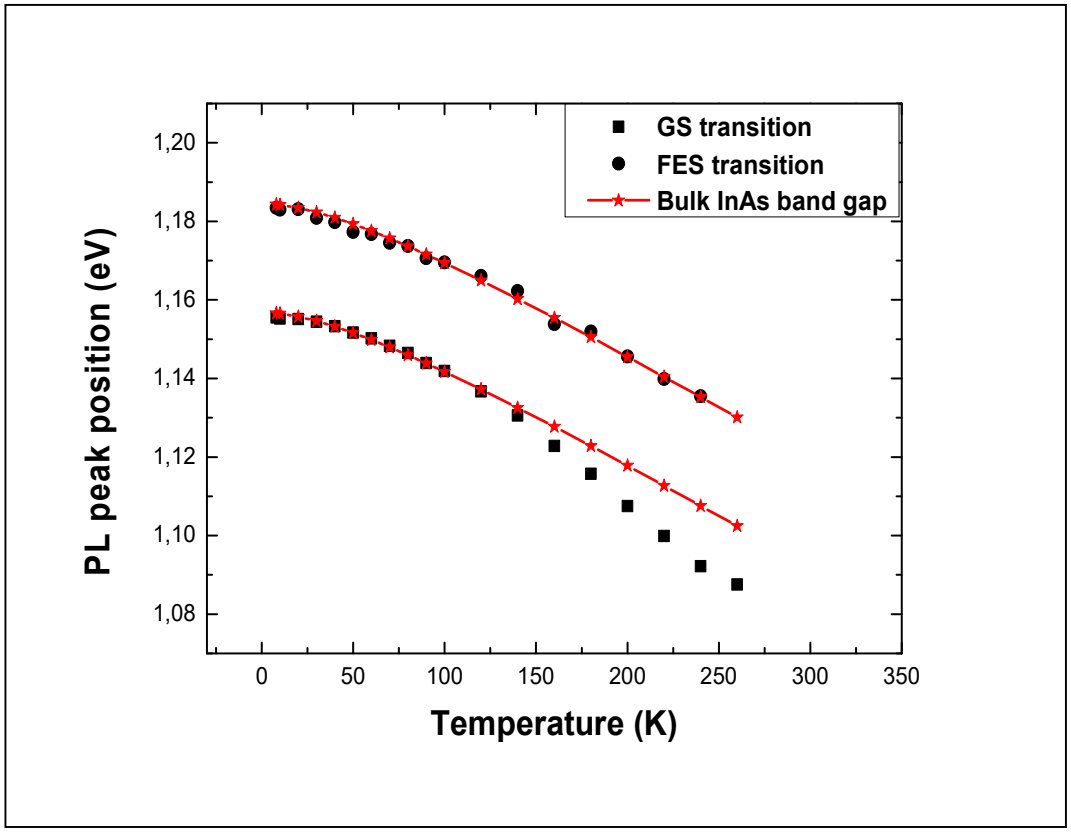
GS transition
FES transition
Bulk InAs band gap
PL peak position (eV)
1,20
1,18
1,16
1,14
1,12
1,10
1,08
0
50
100
150
200
250
300
350
Temperature (K)

Figure 4a

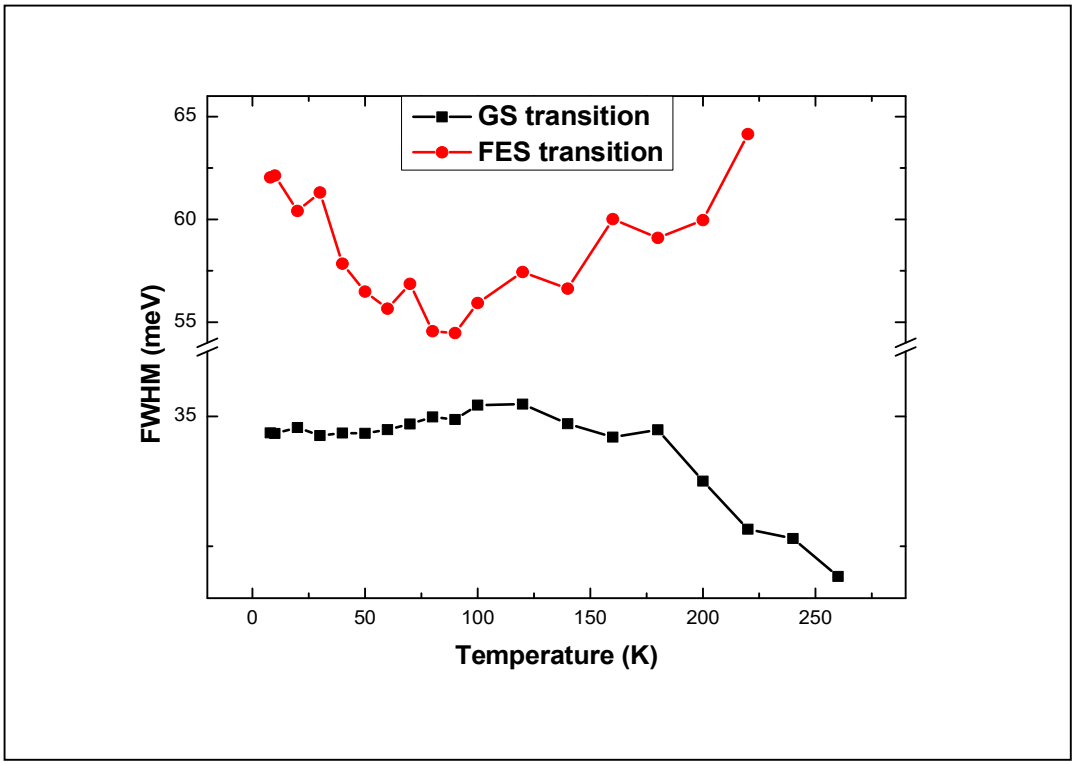
GS transition
FES transition
FWHM (meV)
65
60
55
35
0
50
100
150
200
250
Temperature (K)

Figure 4b

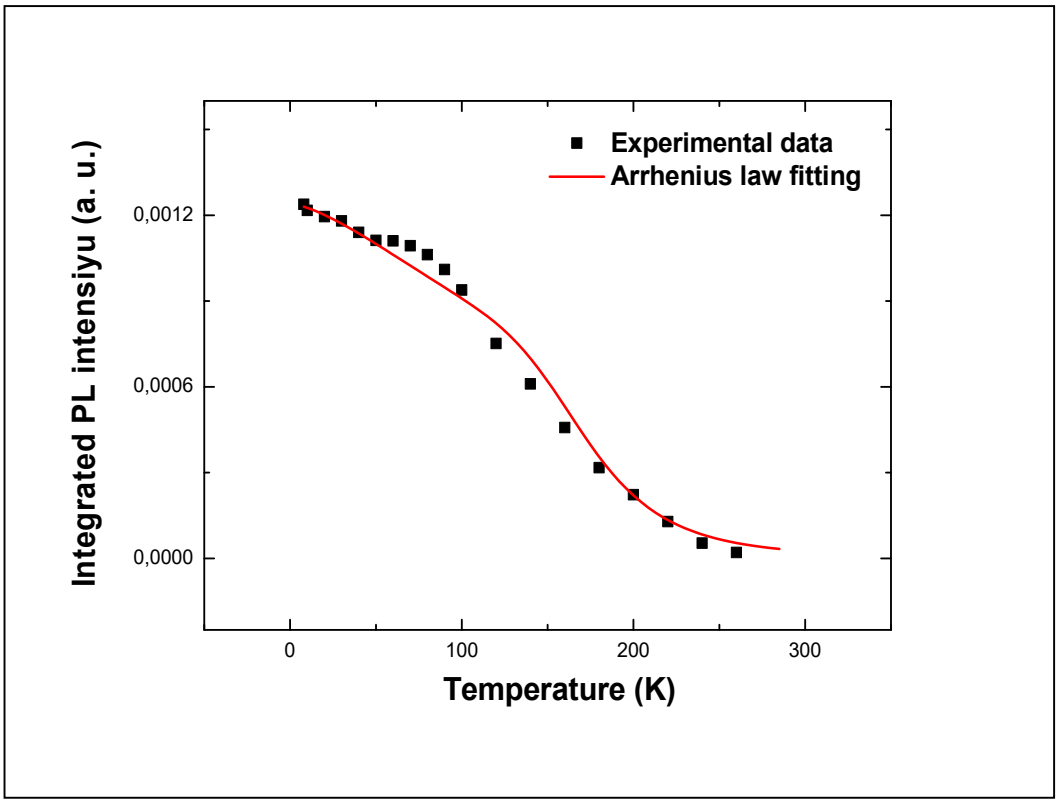
Experimental data
Arrhenius law fitting
Integrated PL intensiyu (a. u.)
0,0012
0,0006
0,0000
0
100
200
300
Temperature (K)

Figure 4c

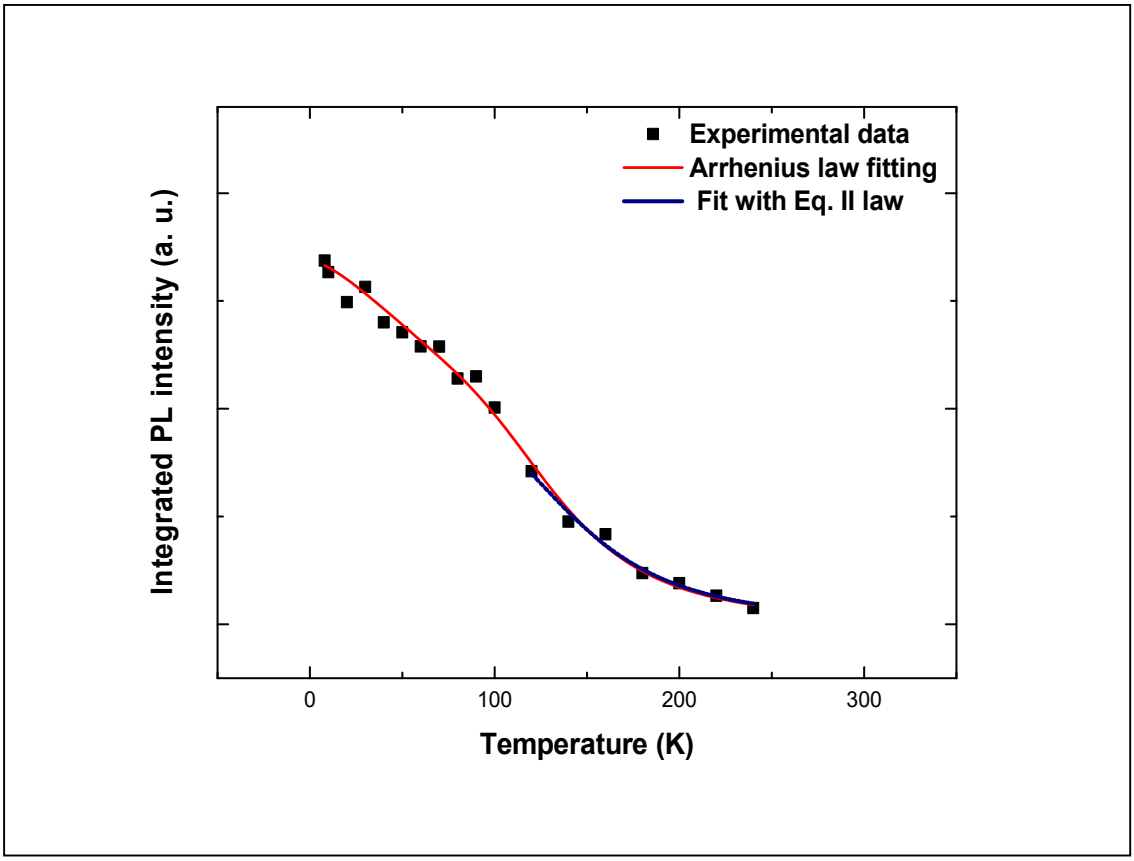
Experimental data
Arrhenius law fitting
Fit with Eq. II law
Integrated PL intensity (a. u.)
0
100
200
300
Temperature (K)

Figure 4d

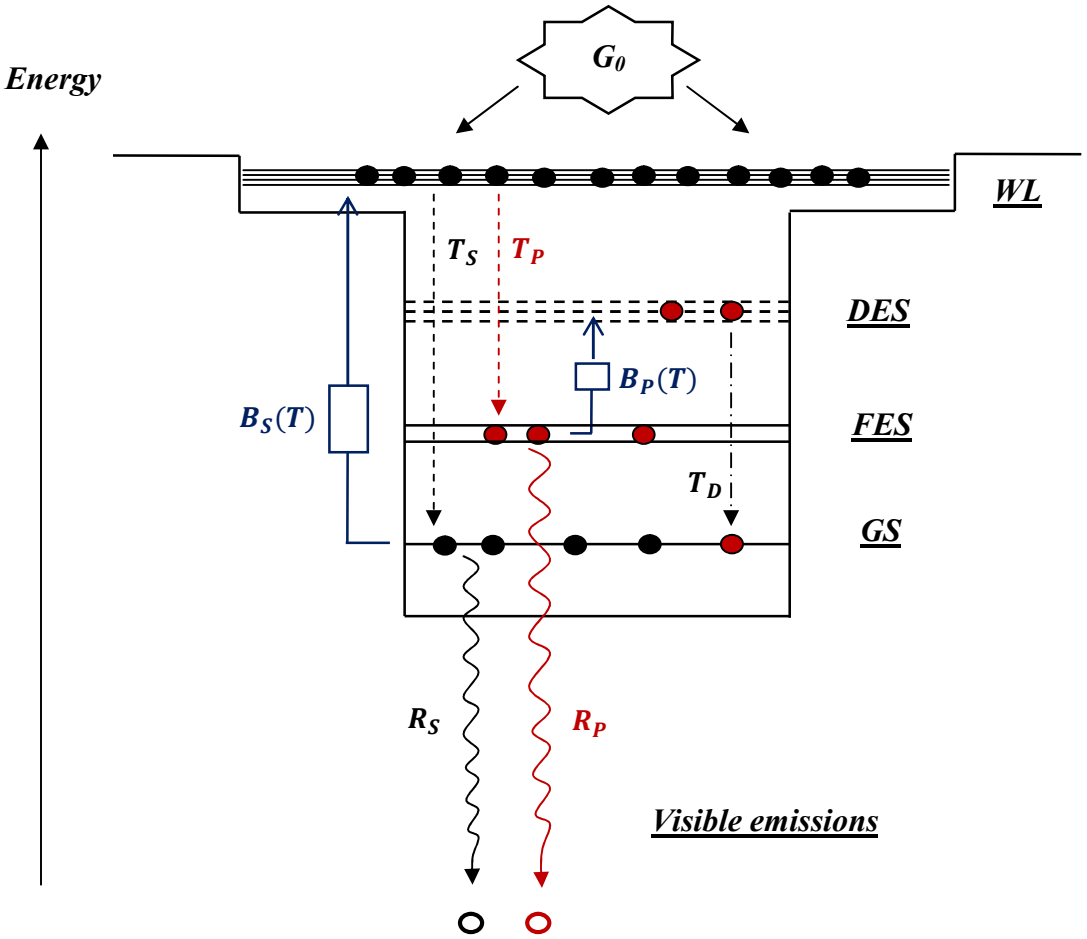
Energy
G_0
WL
T_S
T_P
DES
$B_P(T)$
$B_S(T)$
FES
T_D
GS
R_S
R_P
Visible emissions

Figure 5

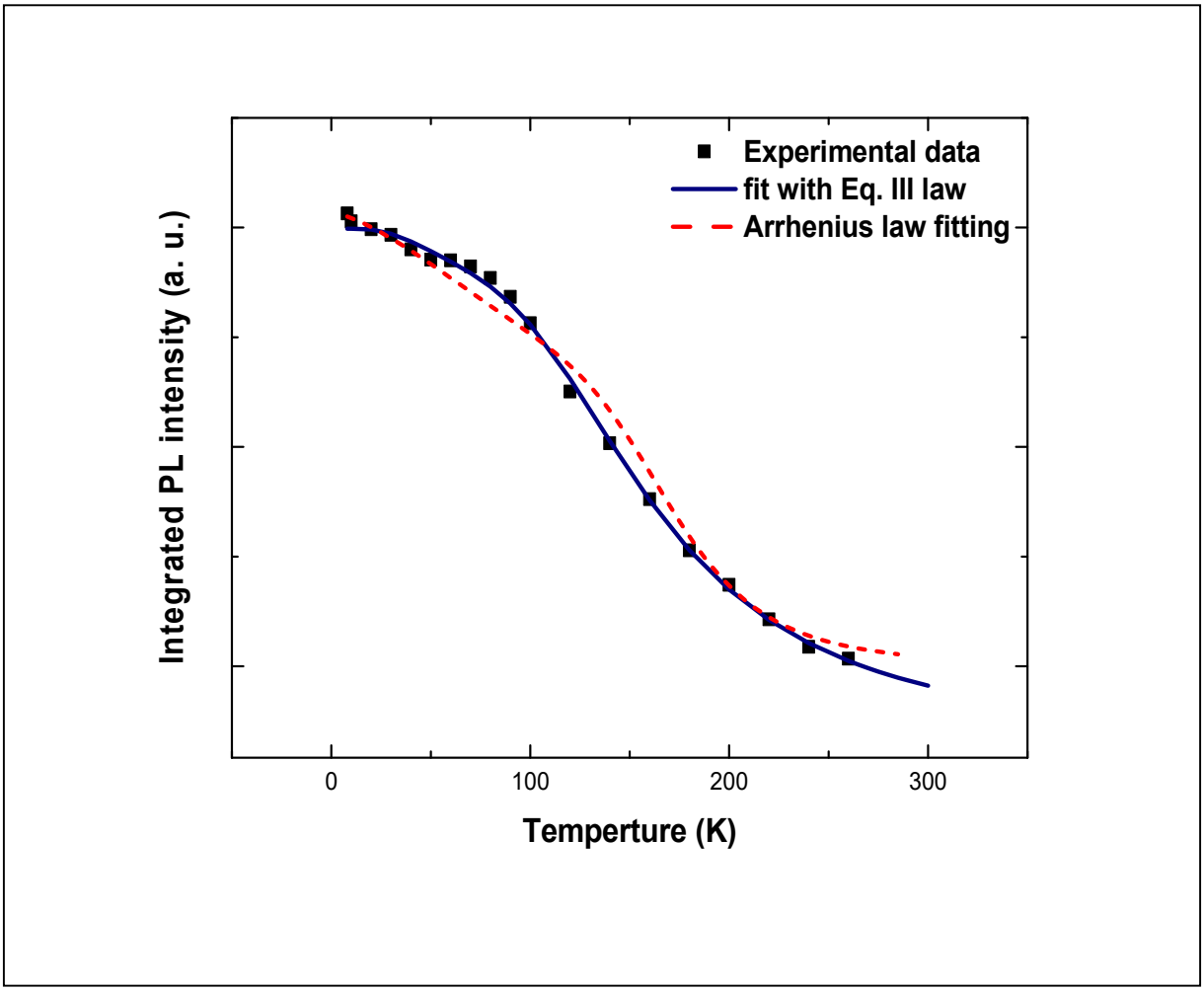
Experimental data
fit with Eq. III law
Arrhenius law fitting
Integrated PL intensity (a. u.)
0
100
200
300
Temperture (K)

Figure 6